Electronic Supplementary Material (ESI) for Molecular Systems Design & Engineering.

Supporting Information

Electrochemically mediated deionization: a review

Adarsh Suresh[1*], Grant T. Hill[1*], Eli Hoenig[1*], Chong Liu[1†]

[1]Pritzker School of Molecular Engineering, University of Chicago, 5640 S Ellis Ave, Chicago, IL 60637

[†]Correspondence should be addressed to C.L. (chongliu@uchicago.edu)

[*]These authors contributed equally. The sequence appears as a result of flip coins outcomes.

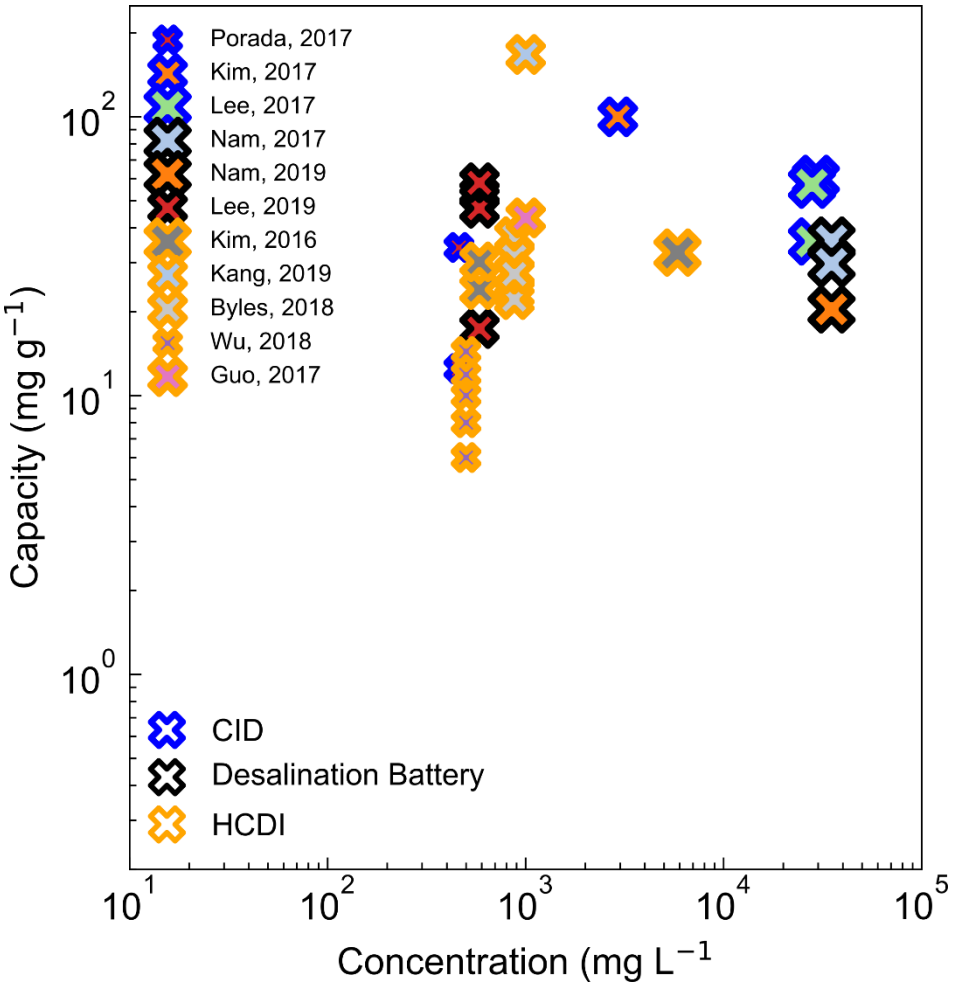

Fig. S1: Capacity vs Concentration plot for faradaic insertion mechanisms wherein there is no observed linear relationship as with capacitive mechanisms (Fig. 2c of the main text)

Citation	Material Class	Material	Feed Conc. mg L^{-1}	Feed Flow Rate ml min^{-1}	Constant Voltage V	Capacity mg g^{-1}	Average Ion Removal Rate mg g^{-1} min^{-1}	Max Ion Removal Rate mg g^{-1} min^{-1}
Wang, 2012[1]	Hierarchical carbon	Electrospun carbon fiber	90	5.0	1.6	9.1	0.08	0.24
Li, 2012[2]	2D material	rGO activated carbon composite	36	25.0	2	0.4	0.02	0.04
Chen, 2018[3]	Mesoporous carbon	Ordered Mesoporous Carbon	500	20.0	1.2	10.8	0.12	0.20
Yeh, 2015[4]	Activated carbon	Activated Carbon	29	5.0	1	9.7	0.26	0.45
Liu, 2020[5]	Hierarchical carbon	Block copolymer fibers	500	0.0	1	30.4	4.42	38.00
Xu, 2019[6]	mesoporous carbon	N-doped mesostructured carbon	584	20.0	1.2	20.6	1.10	2.33
Li, 2009[7]	mesoporous carbon	Hydrated Nickel Sulfate derived ordered mesoporous carbons	47	20.0	0.8	0.9	0.10	0.12
Zhao, 2016[8]	hierarchical carbon	N-doped porous carbon	361	40.0	1.4	13.0	0.33	1.80
Gao, 2019[9]	mesoporous carbon	Mesoporous carbon	250	34.0	1.2	4.8	0.05	0.31
Jia, 2018[10]	2D material	Defect-rich MoS2 sheets	100	-	0.8	24.6	0.49	0.71
Xing, 2017[11]	2D material	ce-MoS2	400	-	1.2	8.8	0.32	0.82
Han, 2020[12]	2D material	N,P-co-doped three-dimensional graphene	800	15.0	1.6	20.9	0.42	0.80
Dianbudiyanto, 2019[13]	2D material	hierarchically porous 3D architectural graphene	500	20.0	1.4	21.6	1.25	1.45
Zhang, 2020[14]	hierarchical carbon	α-cellulose derived hierarchically porous carbon	1000	30.0	1.2	83.0	11.80	17.90
Xu, 2017[15]	activated carbon	Biomass (Pomelo peel) derived N,P-co-doped Meso-/microporous Carbon	1000	40.0	1.2	20.8	0.52	3.30

Zornitta, 2017[16]	activated carbon	Polyanaline serived activated carbon	600	26.0	1.4	14.9	1.08	2.43
Hsu, 2020[17]	activated carbon	Nitrogen-doped activated carbon (NAC)	468	30.0	1.2	24.7	0.15	2.55
Luo, 2017[18]	Mesoporous carbon	Carbon aerogels derived from polyacrylonitrile incorporated with graphene oxide sheets	500	25.0	1.2	15.7	3.80	14.36
Liu, 2013[19]	Mesoporous carbon	Carbon aerogels electrodes with reduced graphene oxide additive	72	40.0	1.2	-	0.33	0.91
Liu, 2019[20]	hierarchical carbon	Chitosan derived nitrogen doped hierarchically porous carbon	500	25.0	1.2	17.9	0.71	2.81
Li, 2009[21]	2D material	Graphene	36	40.0	2	1.9		
Li, 2010[22]	2D material	Graphene-like nanoflakes	25	25.0	2	0.0	0.37	0.43
Yang, 2014[23]		Sponge templated graphene	77	3.0	1.5	5.0		
Wang, 2013[24]	Macroporous Carbon	Macroporous 3D graphene	78	25.0	1.6	3.9	0.24	1.06
Hu, 2017[25]	hierarchical carbon	Polymerized High Internal Phase Emulsion (PolyHIPE) derived Hierarchically Porous carbon	500	100.0	1.2	21.3	1.76	6.00
Li, 2010[26]	Carbon Nanotube	carbon nanotubes/carbon nanofibers composite electrodes	500	-	1.2	16.3	0.11	0.51
Wang, 2011[27]	Carbon Nanotube	Carbon nanotube sponge	60	-	1.2	4.3	0.01	0.05
Aldalbahi, 2018[28]	Carbon Nanotube	Single-walled CNT/porous reticulated vitreous carbon	75	50.0	1.1	3.2	0.60	1.71
Xu, 2015[29]	Carbon Nanotube	Graphene/CNT hybrid sponge	500	27.0	1.2	18.7	1.79	5.28
Wang, 2007[30]	Carbon Nanotube	Carbon nanotubes	500	-	1.2	2.5	0.04	0.11

Belaustegui, 2018[31]	Carbon nanofiber	N -doped PAN -derived carbon nanofibers	585	7.7	1.2	20.0	1.13	3.98
Zhu, 2018[32]	Carbon nanofiber	N -doped bacterial cellulose derived porous carbon nanofiber aerogel	1000	20.0	1.2	17.3	0.92	4.78
Li, 2018[33]	Mesoporous carbon	Phosphorus-doped 3D carbon nanofiber aerogels derived from bacterial-cellulose	1000	50.0	1.2	16.2	0.26	13.94
Liu, 2014[34]	Carbon nanofiber	ZnCl2 activated electrospun carbon nanofiber	500	10.0	1.2	10.5	0.18	0.32
Yin, 2013[35]	2D material	Three-Dimensional Graphene/Metal Oxide Nanoparticle Hybrids	500	-	1.2	15.1	3.35	13.55
Khan, 2018[36]	2D material	3D intercalated graphene sheet -sphere nanocomposite	500	20.0	1.2	20.4	0.31	1.83
Yan, 2018[37]	2D material	Sandwich-like nitrogen -doped graphene composite	500	-	1.2	18.4	0.30	1.87
Xu, 2015[38]	2D material	Nitrogen doped graphene sponge	500	27.0	1.2	21.0	0.25	0.96
Wang, 2017[39]	2D material	Nitrogen-doped carbon/graphene nano-sandwiches	589	100.0	1.2	17.5	2.60	3.53
Zhang, 2018[40]	hierarchical carbon	Zwitterionic Polymer Modified Porous Carbon	245	10.0	1.2	16.5	3.30	16.95
Liu, 2015[41]	hierarchical carbon	Nitrogen-doped porous carbon spheres	1000	50.0	1.2	14.9	0.88	3.89
Feng, 2018[42]	hierarchical carbon	Highly porous activated carbon with multi-channeled structure	585	5.0	1	22.5	0.38	1.64
Zhang, 2018[43]	hierarchical carbon	N, P, S co-doped hollow carbon polyhedra	500	50.0	1.2	22.2	0.26	0.50

Citation	Cell Class	Cell Configuration	Material	Feed Conc. mg L^{-1}	Feed Flow Rate mL min^{-1}	Constant Current mA cm^{-2}	Constant Voltage V	Capacity mg g^{-1}	Average Ion Removal Rate mg g^{-1} s^{-1}	Specific Energy Consumption
Pasta, 2012[44]	Desalination Battery	Batch	$Na_2Mn_5O_{10}$ nanorod/AgCl	11250 (K, Mg, Ca SO_4 present)	-	0.5	-	0.885 mg cm^{-2}	0.000380 mg cm^{-2} s^{-1}	0.290 kWh m^{-3}
Nam, 2017[45]	Desalination Battery	Batch, undivided cell	$NaTi_2(PO_4)_3$/Bi – Pt/Bi	35100	-	1.0	-	-	-	57.3 kWh m^{-3} Cl^- 19.1 kWh m^{-3} Na^+
	Desalination Battery	Batch, divided cell: acidic on Bi side	$NaTi_2(PO_4)_3$/Bi – Pt/Bi	35100	-	1.0	-	36.0	0.0372	5.90 kWh m^{-3} Cl^- ,2.00 kWh m^{-3} Na^+
	Desalination Battery	Batch, divided cell: acidic on Bi side	$NaTi_2(PO_4)_3$/Bi – Pt/Bi	35100	-	2.0	-	29.7	0.0745	-
Nam, 2019[46]	Desalination Battery	Batch, neutral desalination, acidic salination	CuHCF–*n*H_2O/Bi –Pt/Bi	35100	-	1.0	-	20.4	0.0231	9.90 kWh m^{-3} Cl^- 3.90 kWh m^{-3} Na^+
Lee, 2019[47]	Desalination Battery	Flow with AEM and CEM. Side channel conc. 10 mM NaCl	NaNiHCF/Ag	584	5.0	-	1.0	17.4	0.0145	-
	Desalination Battery	side conc. 1000 mM NaCl	NaNiHCF/Ag	584	5.0	-	1.0	52.9	0.0441	-
	Desalination Battery	side conc. 1000 mM NaCl	NaNiHCF/Ag	584	5.0	-	0.8	47.0	0.0392	78.7 kJ mol^{-1}
	Desalination Battery	side conc. 1000 mM NaCl	NaNiHCF/Ag	584	5.0	-	1.2	58.0	0.0483	112 kJ mol^{-1}
	Desalination Battery	side conc. 10	NaNiHCF/Ag	584	5.0	1.0	-	25.7	-	-

	Desalination Battery	side conc. 1000	NaNiHCF/Ag	584	5.0	1.0	-	52.8	-	-
	Desalination Battery	side conc. 10	NaNiHCF/Ag	584	5.0	1.5	-	8.5	-	-
	Desalination Battery	side conc. 1000	NaNiHCF/Ag	584	5.0	4.0	-	34.1	-	-
Kim, 2016[48]	Hybrid CDI	Flow with AEM	$Na_2FeP_2O_7$/ AC	584	2.0	-	1.2	30.2	0.0336	-
	Hybrid CDI	Flow with AEM	$Na_2FeP_2O_7$/ AC	5840	2.0	-	1.2	32.6	0.0362	-
	Hybrid CDI	Flow with AEM	$Na_2FeP_2O_7$/ AC	584	2.0	1.0	-	24.0	0.0220	-
	Hybrid CDI	Flow with AEM	$Na_2FeP_2O_7$/ AC	584	2.0	1.5	-	-	0.0340	-
	Hybrid CDI	Flow with AEM	$Na_2FeP_2O_7$/ AC	584	2.0	2.0	-	-	0.0500	-
	Hybrid CDI	Flow with AEM	$Na_2FeP_2O_7$/ AC	584	2.0	3.0	-	-	0.0700	-
Guo, 2017[49]	Hybrid CDI	Flow with AEM	PB@NPG/AC	1000	650	0.3	-	120	-	16.8 kJ mol^{-1}
	Hybrid CDI	Flow with AEM	PB@NPG/AC	1000	650	0.4	-	86.2	-	-
	Hybrid CDI	Flow with AEM	PB@NPG/AC	1000	650	1.0	-	43.4	0.293	-
	Hybrid CDI	Flow with AEM	PB@NPG/AC		650	2.0	-	-	0.543	-
	Hybrid CDI	Flow with AEM	PB@NPG/AC	10000	650	1.0	-	83.3	-	-
Byles, 2018[50]	Hybrid CDI	Flow with AEM and CEM	α–MnO_2/AC	877	20	-	1.2	22.1	0.0246	-
	Hybrid CDI	Flow with AEM and CEM	Tod–MnO_2/AC	877	20	-	1.2	23.3	0.0259	-
	Hybrid CDI	Flow with AEM and CEM	2 *x* n–MnO_2/ AC	877	20	-	1.2	27.8	0.0309	-
	Hybrid CDI	Flow with AEM and CEM	Hybrid–MnO2/ AC	877	20	-	1.2	27.3	0.0303	-

Wu, 2018[51]	Hybrid CDI	Flow	MnO_2/ AC-QPVP	500	9.2	-	0.6	6.00	0.0200	-
	Hybrid CDI	Flow	MnO_2/ AC-QPVP	500	9.2	-	0.8	8.00	0.0267	-
	Hybrid CDI	Flow	MnO_2/ AC-QPVP	500	9.2	-	1.0	10.0	0.0333	-
	Hybrid CDI	Flow	MnO_2/ AC-QPVP	500	9.2	-	1.2	11.9	0.0397	-
	Hybrid CDI	Flow	MnO_2/ AC-QPVP	500	9.2	-	1.4	14.4	0.0480	-
Byles, 2018[52]	Hybrid CDI	Flow with AEM and CEM	Na-birnessite/ AC	877 NaCl	20	-	1.2	31.5	0.0350	-
	Hybrid CDI	Flow with AEM and CEM	Na-birnessite/ AC	1430 $MgCl_2$	20	-	1.2	50.2	0.0558	-
	Hybrid CDI	Flow with AEM and CEM	Mg-buserite/ AC	877 NaCl	20	-	1.2	37.2	0.0413	-
	Hybrid CDI	Flow with AEM and CEM	Mg-buserite/ AC	1430 $MgCl_2$	20	-	1.2	39	0.0433	-
Wang, 2019[53]	Hybrid CDI	Flow with AEM and CEM	$NaTi_2(PO_4)_3$/ C	1000	100	-	1.8	167.4	0.093	-
Smith, 2016[54]	CID (Simulation)	Flow with AEM	$Na_{0.44}MnO_2$/ $NaTi_2(PO_4)_3$ simulation	40900	-	7.7	-	-	-	2.00–2.30 kWh m^{-3}
	CID (Simulation)	Flow with AEM	$Na_{0.44}MnO_2$/ $NaTi_2(PO_4)_3$ simulation	40900	-	1.3	-	-	-	0.700–0.900 kJ mol^{-1}
Lee, 2017[55]	CID	Batch with AEM	NaNiHCF/ NaFeHCF	27900 (K, Mg, Ca present)	-	0.5	-	57.1	0.0159	0.340 kWh m^{-3}
	CID	Batch with AEM	NaNiHCF/ NaFeHCF	27900	-	0.5	-	35.7	0.0149	0.140 kWh m^{-3}
	CID	Batch with AEM	NaNiHCF/ NaFeHCF	29200	-	0.5	-	59.9	0.0166	-
Kim, 2017[56]	CID	Flow cell with AEM (single)	NaCuHCF/ CuFeHCF	2920	0.5	1.0	-	7.00 mM NaCl	-	-

	CID	Flow cell with AEM (single)	NaCuHCF/ CuFeHCF	2920	0.5	0.6	-	4.00 mM	0.00800 mM s^{-1}	-
	CID	Flow cell with two AEM and one CEM (double)	NaCuHCF/ CuFeHCF	2920	0.5	0.6	-	8.00 mM	0.0160 mM s^{-1}	-
	CID	Flow cell with three AEM and two CEM (triple)	NaCuHCF/ CuFeHCF	2920	0.5	0.6	-	12.0 mM	0.0240 mM s^{-1}	-
	CID	Flow cell with three AEM and two CEM (triple)	NaCuHCF/ CuFeHCF	2920	0.5	0.3	-	100	0.100	-
	CID	Flow cell with three AEM and two CEM (triple)	NaCuHCF/ CuFeHCF	1460	0.5	0.6	-	8.00 mM	-	2.10 kJ mol^{-1} 0.020 kWh m^{-3}
	CID	Two double flow cells in series	NaCuHCF/ CuFeHCF	1990	0.5	0.6		17.0 mM	-	14.7 kJ mol^{-1} 0.070 kWh m^{-3}
	CID	Two double flow cells in series with recycle	NaCuHCF/ CuFeHCF	2920	0.5	0.6	-	33.0 mM	-	71.5 kJ mol^{-1} 0.160 kWh m^{-3}
Porada, 2017[57]	CID	Flow with AEM	NiHCF/NiHCF	460	10	0.28	-	12.5	0.00250	~60.0 kJ mol^{-1}
	CID	Flow with AEM	NiHCF/NiHCF	460	10	0.14	-	12.5	0.00120	~15.0 kJ mol^{-1}
	CID	Flow with AEM	NiHCF/NiHCF	460	10	0.28	-	34.0	0.00250	
Ahn, 2020[58]	CID (anion)	Batch with AEM and CEM	Ag/AgCl	29200	-	1.0	-	85.0	-	5.30 kJ mol^{-1} 0.190 kWh m^{-3}
	CID	Batch with AEM and CEM	Ag/AgCl	58400	-	3.0	-	130	-	
Desai, 2018[59]	Redox Flow	Flow with AEM and CEM	Zn/Zn^{2+} (anolyte) ($[Fe(CN)_6]^{4-}$ /$[Fe(CN)_6]^{3-}$) (catholyte)	35000	10	0.7 - desalination 1.3 - salination	-	30.2 g L^{-1}	--	14.7 kJ mol^{-1} 2.11 kWh m^{-3}
	Redox Flow	Flow with AEM and CEM	Zn/Zn^{2+} (anolyte)	100000	10	1.3 - desalination	-	86.6 g L^{-1}	-	12.7 kWh m^{-3}

			($[Fe(CN)_6]^{4-}$ /$[Fe(CN)_6]^{3-}$) (catholyte)			2.5 - salination				
	Redox Flow	Batch with AEM and CEM	Zn/Zn^{2+} (anolyte) ($[Fe(CN)_6]^{4-}$ /$[Fe(CN)_6]^{3-}$) (catholyte)	35000	-	0.7 - desalination 1.3 - salination	-	14.0 g L^{-1}	0.324 mg L^{-1} s-1	1.63 kWh m^{-3}
	Redox Flow	Batch with AEM and CEM	Zn/Zn^{2+} (anolyte) ($[Fe(CN)_6]^{4-}$ /$[Fe(CN)_6]^{3-}$) (catholyte)	35000	-	Redox Flow	-	21.0 g L^{-1}	0.324 mg L^{-1} s^{-1}	2.19 kWh m^{-3}
Beh, 2019[60]	Redox Flow	Flow with two AEM and one CEM	$Na_4Fe(CN)_6$/ $K_3Fe(CN)_6$	36000	100	-	0.5	35.7 g L^{-1}	14.5 mg L^{-1} s^{-1}	48.8 kJ mol^{-1} 8.80 kWh m^{-3}
	Redox Flow	Flow with two AEM and one CEM	$(BTMAP\text{-}Fc)^{+}$/ (BTMAP-Fc)	35000	100	-	0.5	34.8 g L^{-1}	10.5 mg L^{-1} s^{-1}	52.6 kJ mol^{-1} 10.4 kWh m^{-3}
	Redox Flow	Flow with two AEM and one CEM	$(BTMAP\text{-}Fc)^{+}$/ (BTMAP-Fc)	35000	100	-	0.2 -> 0.5	34.8 g L^{-1}	-	4.93 kWh m^{-3}
	Redox Flow	Flow with two AEM and one CEM	$(BTMAP\text{-}Fc)^{+}$/ (BTMAP-Fc)	35000	100	-	0.1	34.5 g L^{-1}	-	9.68 kJ mol^{-1} 1.58 kWh m^{-3}
	Redox Flow	Batch mode with 7 stages	VCl_3/VCl_2 (anolyte) NaI/NaI_3 (catholyte)	204000	-	-	stages 1-6: 0.2 V; stage 7: 0.2 V until 3.0 g/L then 0.5 V until end	203 g L^{-1}	-	84.4 kWh m^{-3}
Hou, 2018[61]	Redox Flow	Flow AEM and CEM	VCl_3/VCl_2 (anolyte) NaI/NaI_3 (catholyte)	19000	30	0.22	-	0.400 g L^{-1}	-	10.3 kJ mol^{-1}

	Redox Flow	Flow AEM and CEM	VCl_3/VCl_2 (anolyte) NaI/NaI_3 (catholyte)	19000	30	0.44	-	0.300 g L^{-1}	-	-
	Redox Flow	Flow AEM and CEM	VCl_3/VCl_2 (anolyte) NaI/NaI_3 (catholyte)	19000	30	0.88	-	0.100 g L^{-1}	-	-

Table S2. Desalination Performance for Faradaic Desalination Technology in the Literature

Term	Acronym
Seawater reverse osmosis	SWRO
Electrodialysis	ED
Electrical double layer	EDL
Ion exchange membrane	IEM
Cation exchange membrane	CEM
Anion exchange membrane	AEM
Capacitive deionization	CDI
Membrane capacitive deionization	MCDI
Hybrid capacitive deionization	HCDI
Cation insertion desalination	CID
Shock electrodialysis	SED
Flow electrode capacitive deionization	FCDI
Guoy-Chapman-Stern	GCS
Modified Donnan	mD
Ion depletion zone	IDZ
Half-wave rectified alternating current electrochemical method	HW-ACE
Direct current	DC
Alternating current	AC
Asymmetrical alternating current electrochemistry	AACE
California Human Health Screening Levels	CHHSL
Ethylenediaminetetraacetic acid	EDTA
Poly(amidoxime) modified carbon electrode	C-Ami
Graphene-oxide-modified carbon felt electrode	C-rGO

Poly(amidoxime) modified carbon felt electrode	PACCF
Carbon nanotube	CNT
Polypyrrole	PPy
Polypyrrole modified carbon nanotubes	PPy-CNT
Poly(4-vinylpyridine)	P4VP
Polyanaline	PANI
Polyacetylene	PA
Poly(3,4-ethylenedioxythiophene):Poly(4-styrenesulfonate)	PEDOT:PSS
Polyvinylferrocene	PVF
Polyvinylferrocene modified carbon nanotubes	PVF-CNT
Poly(2,6-pyridinedicarboxylicacid)	PDDA
Density functional theory	DFT

Table S3. Common electrochemical deionization terms and corresponding acronyms

Metric	Acronym	Unit	
Salt adsorption capacity	SAC	mg g^{-1}	mg L^{-1}
Average salt adsorption rate	ASAR	mg g^{-1} min^{-1}	mg L^{-1} min^{-1}
Maximum salt adsorption capacity	Eq-SAC	mg g^{-1}	
Charge efficiency	Λcycle	%	
Coulombic efficiency	ηcoul	%	
Energy-normalized adsorbed salt	ENAS	umol J^{-1}	
Mass of electrode	m	g	
Molar mass of feed stream salt	M	g mol^{-1}	
Applied current during charging/discharging	I	mA	
Applied voltage during charging/discharging	V	V	
Salt removal fraction		%	
Specific capacitance		F g^{-1}	F cm^{-2}
Volumetric specific energy consumption	SEC-v	kWh m^{-3}	
Molar specific energy consumption	SEC-m	kJ mol^{-1}	
Gravimetric specific energy consumption	SEC-1	J^{-1} mg	
Capacity retention for number of cycles		%	
Round-trip efficiency		%	
Water recovery percentage	WR	%	
Volume of desalinated water	V	mL	
Concentration of feed stream	Cfeed	mM	mg L^{-1}
Volumetric flowrate	Q	ml min^{-1}	

Productivity	P	$L\ h^{-1}\ m^{-2}$	
Measured feed water electrical conductivity	k	$mS\ cm^{-1}$	
Electrical conductivity		$S\ cm^{-1}$	
Specific surface area	SSA	$m^2\ g^{-1}$	
Diffusion coefficient	D	$cm^2\ s^{-1}$	

Table S4. Common electrochemical deionization performance metrics and corresponding acronyms/units

1. Wang, G. *et al.* Hierarchical activated carbon nanofiber webs with tuned structure fabricated by electrospinning for capacitive deionization. *J. Mater. Chem.* **22**, 21819–21823 (2012).
2. Li, H., Pan, L., Nie, C., Liu, Y. & Sun, Z. Reduced graphene oxide and activated carbon composites for capacitive deionization. *J. Mater. Chem.* **22**, 15556–15561 (2012).
3. Chen, Z. *et al.* A study of the effect of carbon characteristics on capacitive deionization (CDI) performance. *Desalination* **433**, 68–74 (2018).
4. Yeh, C.-L., Hsi, H.-C., Li, K.-C. & Hou, C.-H. Improved performance in capacitive deionization of activated carbon electrodes with a tunable mesopore and micropore ratio. *Desalination* **367**, 60–68 (2015).
5. Liu, T. *et al.* Exceptional capacitive deionization rate and capacity by block copolymer–based porous carbon fibers. *Science Advances* **6**, eaaz0906 (2020).
6. Xu, X. *et al.* Capacitive deionization using nitrogen-doped mesostructured carbons for highly efficient brackish water desalination. *Chemical Engineering Journal* **362**, 887–896 (2019).
7. Li, L., Zou, L., Song, H. & Morris, G. Ordered mesoporous carbons synthesized by a modified sol–gel process for electrosorptive removal of sodium chloride. *Carbon* **47**, 775–781 (2009).
8. Zhao, S. *et al.* High capacity and high rate capability of nitrogen-doped porous hollow carbon spheres for capacitive deionization. *Applied Surface Science* **369**, 460–469 (2016).

9. Gao, T. *et al.* Mesoporous carbon derived from ZIF-8 for high efficient electrosorption. *Desalination* **451**, 133–138 (2019).
10. Jia, F. *et al.* Defect-rich molybdenum disulfide as electrode for enhanced capacitive deionization from water. *Desalination* **446**, 21–30 (2018).
11. Xing, F. *et al.* Chemically exfoliated MoS_2 for capacitive deionization of saline water. *Nano Energy* **31**, 590–595 (2017).
12. Han, D.-C. *et al.* High-performance capacitive deionization using nitrogen and phosphorus-doped three-dimensional graphene with tunable pore size. *Electrochimica Acta* **336**, 135639 (2020).
13. Dianbudiyanto, W. & Liu, S.-H. Outstanding performance of capacitive deionization by a hierarchically porous 3D architectural graphene. *Desalination* **468**, 114069 (2019).
14. Zhang, P., Li, J. & Chan-Park, M. B. Hierarchical Porous Carbon for High-Performance Capacitive Desalination of Brackish Water. *ACS Sustainable Chem. Eng.* **8**, 9291–9300 (2020).
15. Xu, D., Tong, Y., Yan, T., Shi, L. & Zhang, D. N,P-Codoped Meso-/Microporous Carbon Derived from Biomass Materials via a Dual-Activation Strategy as High-Performance Electrodes for Deionization Capacitors. *ACS Sustainable Chem. Eng.* **5**, 5810–5819 (2017).
16. Zornitta, R. L. *et al.* High-performance activated carbon from polyaniline for capacitive deionization. *Carbon* **123**, 318–333 (2017).

17. Hsu, C.-C., Tu, Y.-H., Yang, Y.-H., Wang, J.-A. & Hu, C.-C. Improved performance and long-term stability of activated carbon doped with nitrogen for capacitive deionization. *Desalination* **481**, 114362 (2020).
18. Luo, G., Wang, Y., Gao, L., Zhang, D. & Lin, T. Graphene bonded carbon nanofiber aerogels with high capacitive deionization capability. *Electrochimica Acta* **260**, 656–663 (2018).
19. Liu, Y. *et al.* Carbon aerogels electrode with reduced graphene oxide additive for capacitive deionization with enhanced performance. *Inorganic Chemistry Frontiers* **1**, 249–255 (2014).
20. Liu, X. *et al.* Nitrogen-doped hierarchical porous carbon aerogel for high-performance capacitive deionization. *Separation and Purification Technology* **224**, 44–50 (2019).
21. Li, H., Lu, T., Pan, L., Zhang, Y. & Sun, Z. Electrosorption behavior of graphene in NaCl solutions. *J. Mater. Chem.* **19**, 6773–6779 (2009).
22. Li, H., Zou, L., Pan, L. & Sun, Z. Novel graphene-like electrodes for capacitive deionization. *Environ. Sci. Technol.* **44**, 8692–8697 (2010).
23. Yang, Z.-Y. *et al.* Sponge-templated preparation of high surface area graphene with ultrahigh capacitive deionization performance. *Advanced Functional Materials* **24**, 3917–3925 (2014).
24. Wang, H. *et al.* Three-dimensional macroporous graphene architectures as high performance electrodes for capacitive deionization. *Journal of Materials Chemistry A* **1**, 11778–11789 (2013).

25. Hu, W. *et al.* Hierarchically Porous Carbon Derived from PolyHIPE for Supercapacitor and Deionization Applications. *Langmuir* **33**, 13364–13375 (2017).
26. Li, H. *et al.* Kinetics and thermodynamics study for electrosorption of NaCl onto carbon nanotubes and carbon nanofibers electrodes. *Chemical Physics Letters* **485**, 161–166 (2010).
27. Wang, L. *et al.* Capacitive deionization of NaCl solutions using carbon nanotube sponge electrodes. *Journal of Materials Chemistry* **21**, 18295–18299 (2011).
28. Aldalbahi, A., Rahaman, M., Almoiqli, M., Hamedelniel, A. & Alrehaili, A. Single-Walled Carbon Nanotube (SWCNT) Loaded Porous Reticulated Vitreous Carbon (RVC) Electrodes Used in a Capacitive Deionization (CDI) Cell for Effective Desalination. *Nanomaterials* **8**, 527 (2018).
29. Xu, X. *et al.* Rational design and fabrication of graphene/carbon nanotubes hybrid sponge for high-performance capacitive deionization. *J. Mater. Chem. A* **3**, 13418–13425 (2015).
30. Wang, S. *et al.* Equilibrium and kinetic studies on the removal of NaCl from aqueous solutions by electrosorption on carbon nanotube electrodes. *Separation and Purification Technology* **58**, 12–16 (2007).
31. Belaustegui, Y. *et al.* Electro-spun graphene-enriched carbon fibres with high nitrogen-contents for electrochemical water desalination. *Desalination* **428**, 40–49 (2018).
32. Zhu, G., Wang, H., Xu, H. & Zhang, L. Enhanced capacitive deionization by nitrogen-doped porous carbon nanofiber aerogel derived from bacterial-cellulose. *Journal of Electroanalytical Chemistry* **822**, 81–88 (2018).

33. Li, Y. *et al.* Phosphorus-doped 3D carbon nanofiber aerogels derived from bacterial-cellulose for highly-efficient capacitive deionization. *Carbon* **130**, 377–383 (2018).
34. Liu, J. *et al.* ZnCl2 activated electrospun carbon nanofiber for capacitive desalination. *Desalination* **344**, 446–453 (2014).
35. Yin, H. *et al.* Three-Dimensional Graphene/Metal Oxide Nanoparticle Hybrids for High-Performance Capacitive Deionization of Saline Water. *Advanced Materials* **25**, 6270–6276 (2013).
36. Khan, Z. U., Yan, T., Shi, L. & Zhang, D. Improved capacitive deionization by using 3D intercalated graphene sheet–sphere nanocomposite architectures. *Environ. Sci.: Nano* **5**, 980–991 (2018).
37. Yan, T. *et al.* Capacitive deionization of saline water using sandwich-like nitrogen-doped graphene composites via a self-assembling strategy. *Environ. Sci.: Nano* **5**, 2722–2730 (2018).
38. Xu, X., Sun, Z., Chua, D. H. C. & Pan, L. Novel nitrogen doped graphene sponge with ultrahigh capacitive deionization performance. *Scientific Reports* **5**, 11225 (2015).
39. Wang, M. *et al.* High performance capacitive deionization electrodes based on ultrathin nitrogen-doped carbon/graphene nano-sandwiches. *Chem. Commun.* **53**, 10784–10787 (2017).
40. Zhang, P. *et al.* Zwitterionic Polymer Modified Porous Carbon for High-Performance and Antifouling Capacitive Desalination. *ACS Appl. Mater. Interfaces* **10**, 33564–33573 (2018).

41. Liu, Y. *et al.* Nitrogen-doped porous carbon spheres for highly efficient capacitive deionization. *Electrochimica Acta* **158**, 403–409 (2015).
42. Feng, C., Chen, Y.-A., Yu, C.-P. & Hou, C.-H. Highly porous activated carbon with multi-channeled structure derived from loofa sponge as a capacitive electrode material for the deionization of brackish water. *Chemosphere* **208**, 285–293 (2018).
43. Zhang, J. *et al.* N, P, S co-doped hollow carbon polyhedra derived from MOF-based core–shell nanocomposites for capacitive deionization. *J. Mater. Chem. A* **6**, 15245–15252 (2018).
44. Pasta, M., Wessells, C. D., Cui, Y. & La Mantia, F. A desalination battery. *Nano Lett.* **12**, 839–843 (2012).
45. Nam, D.-H. & Choi, K.-S. Bismuth as a New Chloride-Storage Electrode Enabling the Construction of a Practical High Capacity Desalination Battery. *J. Am. Chem. Soc.* **139**, 11055–11063 (2017).
46. Nam, D.-H., Lumley, M. A. & Choi, K.-S. A desalination battery Combining $Cu_3[Fe(CN)_6]_2$ as a Na-storage electrode and Bi as a Cl-storage electrode enabling membrane-free desalination. *Chem. Mater.* **31**, 1460–1468 (2019).
47. Lee, J. *et al.* Enhancement in desalination performance of battery electrodes via improved mass transport using a multichannel flow system. *ACS Appl. Mater. Interfaces* **11**, 36580–36588 (2019).
48. Kim, S., Lee, J., Kim, C. & Yoon, J. $Na_2FeP_2O_7$ as a novel material for hybrid capacitive deionization. *Electrochimica Acta* **203**, 265–271 (2016).

49. Guo, L. *et al.* A Prussian blue anode for high performance electrochemical deionization promoted by the faradaic mechanism. *Nanoscale* **9**, 13305–13312 (2017).

50. Byles, B. W., Cullen, D. A., More, K. L. & Pomerantseva, E. Tunnel structured manganese oxide nanowires as redox active electrodes for hybrid capacitive deionization. *Nano Energy* **44**, 476–488 (2018).

51. Wu, T. *et al.* Highly stable hybrid capacitive deionization with a MnO_2 anode and a positively charged cathode. *Environ. Sci. Technol. Lett.* **5**, 98–102 (2018).

52. Byles, B. W., Hayes-Oberst, B. & Pomerantseva, E. Ion removal performance, structural/compositional dynamics, and electrochemical stability of layered manganese oxide electrodes in hybrid capacitive deionization. *ACS Appl. Mater. Interfaces* **10**, 32313–32322 (2018).

53. Wang, K. *et al.* Metal–organic-frameworks-derived $NaTi_2(PO_4)_3$ /carbon composites for efficient hybrid capacitive deionization. *J. Mater. Chem. A* **7**, 12126–12133 (2019).

54. Smith, K. C. & Dmello, R. Na-ion desalination (NID) enabled by Na-blocking membranes and symmetric Na-intercalation: porous-electrode modeling. *J. Electrochem. Soc.* **163**, A530–A539 (2016).

55. Lee, J., Kim, S. & Yoon, J. Rocking chair desalination battery based on prussian blue electrodes. *ACS Omega* **2**, 1653–1659 (2017).

56. Kim, T., Gorski, C. A. & Logan, B. E. Low energy desalination using battery electrode deionization. *Environ. Sci. Technol. Lett.* **4**, 444–449 (2017).

57. Porada, S., Shrivastava, A., Bukowska, P., Biesheuvel, P. M. & Smith, K. C. Nickel hexacyanoferrate electrodes for continuous cation intercalation desalination of brackish water. *Electrochimica Acta* **255**, 369–378 (2017).
58. Ahn, J. *et al.* High performance electrochemical saline water desalination using silver and silver-chloride electrodes. *Desalination* **476**, 114216 (2020).
59. Desai, D. *et al.* Electrochemical desalination of seawater and hypersaline brines with coupled electricity storage. *ACS Energy Lett.* **3**, 375–379 (2018).
60. Beh, E. S., Benedict, M. A., Desai, D. & Rivest, J. B. A Redox-Shuttled Electrochemical Method for Energy-Efficient Separation of Salt from Water. *ACS Sustainable Chemistry & Engineering* **7**, 13411–13417 (2019).
61. Hou, X. *et al.* Coupling desalination and energy storage with redox flow electrodes. *Nanoscale* **10**, 12308–12314 (2018).